Applied Catalysis B: Environmental 140–141 (2013) 386–395

Contents lists available at SciVerse ScienceDirect

Applied Catalysis B: Environmental

journal homepage: www.elsevier.com/locate/apcatb

Activity and deactivation of catalysts based on zirconium oxide modified with metal chlorides in the MPV reduction of crotonaldehyde

Juan F. Miñambres, Alberto Marinas, José M. Marinas, Francisco J. Urbano *

Department of Organic Chemistry, Campus de Excelencia Internacional CeiA3, University of Córdoba, Campus de Rabanales, Marie Curie Building (Annex), E-14014 Córdoba, Spain

ARTICLE INFO

Article history:
Received 14 January 2013
Received in revised form 11 April 2013
Accepted 15 April 2013
Available online 24 April 2013

Keywords:
Metal chloride modified zirconia catalysts
Meerwein–Ponndorf–Verley reduction
Chemoselective crotonaldehyde reduction
Surface acidity
Catalyst deactivation

ABSTRACT

The Meerwein–Ponndorf–Verley (MPV) reduction of crotonaldehyde to but-2-enol was conducted in the presence of ZrO_2 based catalysts modified by impregnation with gold, cobalt, nickel or zinc chloride. The resulting solids were characterized in depth and used as catalysts in the previous reaction, where they provided high but-2-enol yields at the expense of a considerable loss of activity with time on stream. The catalysts were found to contain both Brønsted and Lewis acid sites active in the reaction. Based on the results, however, the Lewis sites are much more active but undergo much stronger deactivation than the Brønsted sites. Judging by the reactivity and characterization of the spent catalysts, the Brønsted sites are seemingly more selective despite their lower activity. Modifying ZrO_2 with metal chlorides enhanced the surface Lewis acidity although these sites were found to be responsible for the surface deposition of carbonaceous species leading to catalyst deactivation. The presence in the Au/ZrO_2 catalyst of a type of Lewis acid sites that scarcely deactivates in the process might be related to the presence of metallic Au particles interacting with chlorinated species.

1. Introduction

The reduction of carbonyl compounds by hydrogen transfer from an alcohol is known in Organic Chemistry as the Meerwein–Ponndorf–Verley (or MPV) reduction. The presence of a C=C double bond conjugated with the C=O group in α,β-unsaturated carbonyl compounds introduces an additional dimension in the process, namely: the chemoselective reduction of the carbonyl group in the presence of the C=C bond – because the latter is more thermodynamically susceptible to reduction than the former, the preferred reaction product is not the α,β-unsaturated alcohol. However, the selective synthesis of primary and secondary unsaturated alcohols is an important process for the pharmaceutical, fragrance and food aroma industries [1]. Preparing these compounds by hydrogenation in the presence of a supported metal as catalyst is rather a complex task [2]. However, the MPV reduction reaction has proved effective for the selective reduction of the C=O bond in α,β-unsaturated carbonyl compounds to the corresponding unsaturated alcohols [3].

Traditionally, the MPV reaction has been conducted in a homogeneous medium containing an aluminium or zirconium alkoxide [4,5]. The reaction mechanism in a homogeneous phase, which has been thoroughly studied, involves the formation of a six-member cyclic intermediate where both alcohol and carbonyl are coordinated to the metal site in the alkoxide [6–9]. Nevertheless, the last two decades have witnessed an increasing interest in conducting the process in a heterogeneous phase in order to exploit its advantages over homogeneous catalysis in large-scale applications [9].

α,β-Unsaturated carbonyl compounds have been reduced by hydrogen transfer in the presence of a variety of heterogeneous catalysts including magnesium oxides and hydroxides [10–14], zirconium oxides [15,16] and various active components supported on zeolites [9,17,18] and mesoporous materials [19–21] among others [22]. Especially effective among the heterogeneous catalysts used in the MPV reaction is zirconium oxide [23], an amphoteric solid with a high thermal stability and corrosion resistance that possesses oxidizing and reducing properties [24].

The role of acid–base sites in ZrO_2 in the MPV reaction is controversial. Despite the abundance of studies on this topic, no conclusive evidence of the prevalence of either site type in the process exists as yet [9].

Modifying ZrO_2 by impregnation with an active phase alters its surface properties and enhances the intrinsic activity and selectivity of the oxide in the MPV reaction. This has led to impregnated zirconium oxide being the most widely used catalyst for this process.

* Corresponding author. Tel.: +34 957 218638; fax: +34 957 212066.
E-mail address: FJ.Urbano@uco.es (F.J. Urbano).

0926-3373/$ – see front matter © 2013 Elsevier B.V. All rights reserved.
http://dx.doi.org/10.1016/j.apcatb.2013.04.036

Impregnation in methanol is one of the most effective choices for obtaining modified zirconium oxide. Because alcohols and water are mutually soluble, the former can replace water adsorbed on the surface of small catalyst particles and prevent their aggregation. Heating in a hydroalcoholic medium thus provides an effective means for obtaining catalyst particles of a high surface area and small size [25].

The addition of chloride species is known to strengthen Lewis acid sites in aluminium oxides [26]. In this work, we used methanolic impregnation to obtain new Lewis acid sites from M^{n+}–Cl^{-} species deposited on the surface of catalytic solids.

This work was undertaken to improve existing knowledge about the MPV reduction of modified zirconium oxides examined in previous studies [27,28], with special emphasis on the catalyst deactivation. To this end, we examined the effects of impregnating ZrO_2 with gold, cobalt, nickel or zinc chloride.

2. Experimental

2.1. Synthesis of the catalysts

Zirconium oxide was synthesized by dissolving 65 g of zirconium oxychloride octahydrate (Sigma–Aldrich ref. 31670) in milliQ water and adding ammonium hydroxide to pH 9.5 to precipitate the solid. The precipitate was collected by filtration, washed with distilled water to a negative test for chloride (with $AgNO_3$) and dried at 110 °C for subsequent grinding, sieving and calcining at 300 °C for 6 h.

The amount of solid thus obtained was split into five identical portions four of which were impregnated with methanolic solutions of chloroauric acid, cobalt chloride, nickel chloride and zinc chloride, respectively. Therefore, a 1% (w/w) suspension of ZrO_2 in methanol was prepared. Then, metal chlorides were added to obtain a nominal content of 2.0 mmol/g of support according to Rhodes and Brown [25]. Suspensions were subsequently rotaevaporated to eliminate the solvent. Finally, the solids were heated at 150 or 200 °C for 1 h.

The resulting catalysts were designated X/ZrO_2Y, where X denotes the metal from the impregnated chloride and Y the heating temperature – which is only stated where necessary. The catalysts were all stored in topaz bottles and placed in a desiccator to avoid rehydration.

2.2. Characterization of the catalysts

All solids were characterized in depth for textural, structural and surface chemical properties, using various physical, chemical and spectroscopic techniques.

2.2.1. Thermogravimetric analysis (TGA–DTA)

The catalysts were subjected to thermogravimetric and differential thermal analysis on a Setaram SetSys 12 instrument. An amount of 20 mg of sample was placed in an alumina crucible for TGA–DTA analysis and heated at temperatures from 30 to 1000 °C at a rate of 10 °C/min under a stream of synthetic air at 40 mL/min in order to measure weight loss, heat flow and derivative weight loss.

2.2.2. Chemical analysis

XRD of all catalyst were performed on a Siemens D-5000 X-Ray diffractometer, using a cobalt source, Co Kα, and a graphite monochromator. The voltage and current intensity used were 20 kV and 25 mA, respectively. Scans were performed at 0.05° 2θ intervals over the 2θ range from 4° to 75°.

The catalysts were analyzed on a Perkin Elmer ELAN-DRC-e ICP-MS instrument at the Central Research Support Service (SCAI) of the University of Córdoba. Prior to analysis, an amount of 0.1 g of sample was dissolved in 12 mL of a 1:1:1 mixture of H_2O, H_2SO_4 and HF. The resulting solutions were diluted 1000 times in 3% HNO_3 (v/v) in order to bring their concentrations into the measurable range.

Surface chemical properties in the solids calcined at 150 °C were examined by using an EDS Link ISIS X-ray dispersive energy detector connected to a Jeol JSM-6300 SEM-EDX scanning electron microscope. Images were obtained at 600, 1600, 3000 and 25,000 magnification from randomly chosen zones in each solid and averaged.

X-ray photoelectron spectra (XPS) for the solids were recorded from pellets 0.5 mm thick and 4 mm in diameter obtained by pressing and degassing to a pressure below 2×10^{-8} Torr at 150 °C in a pre-analysis chamber in order to remove volatile species. A Leibold–Heraeus LHS10 spectrometer capable of operating below 2×10^{-8} Torr and equipped with an EA-200MD electron analyser furnished with an Al K_α X-ray source ($h\upsilon$ = 1486.6 eV) of 120 W and 30 mA was used for this purpose. The binding energies obtained were corrected by reference to the adventitious carbon C1s signal at 284.6 eV.

Surface area, and pore diameter and type, were determined from nitrogen adsorption–desorption isotherms recorded at its boiling point after degassing at 110 °C at 0.1 Pa of the catalysts on a Micromeritics ASAP-2010 instrument.

All solids were analyzed by FT-Raman spectroscopy with a Renishaw inVia Raman microscope equipped with a Renishaw CCD camera of 578 × 400 pixels and a 1200 l/mm laser source with 633/780 interlining. Spectra were obtained by using an exposure time of 10 s and 5 scans over the Raman shift range 100–1500 cm^{-1}.

2.2.3. Surface acid–base properties of the catalysts

Surface acidity and basicity in the catalysts were determined by thermal programmed desorption (TPD) of probe molecules previously adsorbed on the solids. The probes used were pyridine for acid sites (TPD-PY) and CO_2 for basicity (TPD-CO_2). An amount of 100 mg of sample was placed under an Ar stream flowing at 75 mL/min in a reactor 10 mm in diameter that was placed inside an oven. The Ar stream was used to clean the solids by heating to 150 °C (and also at 200 °C for TPD-PY) at a rate of 10 °C/min and then cooling by thermal inertia to 50 °C. At that point, the surface of the solid was saturated with the probe molecule for 30 min. Pyridine was supplied by bubbling the Ar stream through liquid pyridine at room temperature, and carbon dioxide by passing a 5% CO_2/Ar stream over the samples. The saturation level was controlled by using mass spectrometry to monitor the probe molecule at m/z 79 for pyridine and 44 for CO_2 on a VG Probal Benchtop QMS instrument from ThermoScientific coupled on-line to the reactor. After saturation, excess physisorbed probe substance was removed by passing an Ar stream at 75 mL/min until the monitored mass fell to pre-saturation levels. Then, desorption was started by raising the temperature to 150 or 200 °C at 10 °C/min and holding the final level for 30 min. Desorbed pyridine was quantified against a calibration graph previously constructed from variable injected volumes of pyridine. Similarly, desorbed carbon dioxide was quantified by using a 5% (v/v) CO_2/Ar standard.

The above-described overall acidity study by TPD-PY was supplemented with one by diffuse reflectance infrared (DRIFT) spectroscopy of the pyridine-saturated solids intended to identify the specific types of acid sites present. Measurements were made with an ABB Bomen MB Series IR spectrophotometer equipped with a SpectraTech P/N 0030-100 environmental chamber including a diffuse reflectance device capable of performing 258 scans at 8 cm^{-1} resolution at an adjustable temperature. Prior to analysis, each catalyst was thermally cleaned at the maximum temperature reached during its synthesis (150 or 200 °C) for 30 min. The last few minutes of the thermal treatment were used to record reference spectra.

Table 1
Textural, structural and chemosurface properties of the different catalysts synthesized in the present work. T_G denotes glow exotherm temperature.

Catalyst	BET (m^2/g)	T_G (°C)	Pore Ø (A)	Chemical composition			Surface acidity				Surface basicity	
				Mt/Zr (mole, %)			TPD 150 °C		TPD 200 °C		TPD 150 °C	
				EDX	ICP	XPS	μmol Py/g	μmol Py/m^2	μmol Py/g	μmol Py/m^2	μmol CO_2/g	μmol CO_2/m^2
Au/ZrO_2	195	442	20	11.2	3.7	10.8	6.4	0.033	11.6	0.06	1.3	0.007
Co/ZrO_2	203	447	20	12.7	6.6	6.8	4.9	0.024	17.0	0.084	7.0	0.035
Ni/ZrO_2	201	455	20	8.2	7.9	6.3	8.7	0.043	15.1	0.075	11.5	0.057
Zn/ZrO_2	190	446	20	20.2	15.2	9.8	15.8	0.083	19.5	0.103	9.5	0.05
ZrO_2	237	419	21	–	–	–	3.5	0.015	12.2	0.052	91.3	0.386

The solids were placed under a pyridine-saturated atmosphere in a hood at 50 °C for 30 min to facilitate adsorption of pyridine at acid sites. After saturation, the solids were transferred back to the DRIFT spectrophotometer to record their spectra at 50, 100, 150 and 200 °C – the last temperature was only used with the solids calcined at that level. The spectral region scanned was 1700–1400 cm^{-1}.

2.2.4. Reactivity

The catalysts were used for the chemoselective gas-phase reduction of crotonaldehyde to but-2-enol in the Meerwein–Ponndorf–Verley (MPV) reaction, using propan-2-ol as hydrogen donor. Runs were performed with amounts of 50 mg of the catalysts in a cylindrical reactor 10 cm long × 0.3 cm ID. The reactor was placed in an oven to control the temperature of the process. A Gibson Mod.307 pump was used to introduce a 0.5 M solution of crotonaldehyde in isopropanol at a rate of 1 g/h into a nitrogen flow of 50 mL/min, the mixture being evaporated in an evaporator–mixer at 130 °C. All reactions were performed in duplicate and their results averaged.

Prior to reaction, the catalysts were cleaned with a synthetic air stream passed at 40 mL/min at the reaction temperature for 30 min. Then, the reaction was started by replacing the cleaning stream with the gas stream from the evaporator–mixer. The reaction was monitored by connecting the reactor on-line to an Agilent 7890A gas chromatograph. Separation was effected by a Supelcowax-10 capillary column (30 m × 0.25 mm ID, 0.25 μm film thickness). Reaction products were quantified by using standard solutions of each compound at concentrations from 0.05 to 0.5 M.

2.2.5. Deactivation of the catalysts

After 5 h of reaction, all catalysts were subjected to *in situ* cleaning with an air stream at 40 mL/min at the reaction temperature for 12 h. Then, a second reaction cycle was started by replacing the synthetic air stream with the reactant stream at a constant temperature.

The deactivated catalysts were subsequently characterized as described above to obtain additional information on how their surface physico-chemical properties were affected by the reaction and their potential role in the deactivation process. To this end, the catalysts were subjected to nitrogen adsorption–desorption isotherms to calculate their BET surface, characterized in terms of surface acidity (DRIFT spectroscopy and TPD-PY), examined by XPS and analyzed by TGA on-line connected to a MS under both synthetic air and argon (TGA–MS).

3. Results and discussion

The whole set of the synthesized catalysts was characterized in depth from textural, structural and chemical point of view. Table 1 summarizes the physico-chemical properties of the solids.

3.1. Thermogravimetric analysis

The thermogravimetric profiles for the impregnated catalysts were similar to those for the starting (ZrO_2) solid. The heat flow profile (DTA) exhibited an exothermic peak (glow exotherm) at 410–460 °C in all samples by effect of the phase change in the zirconium oxide from an amorphous state to an increased crystalline order [29]. This phenomenon is strongly influenced by the presence of metals or other components; as a result, the glow exotherm occurred at a different temperature in each catalyst though in all cases the presence of a metal retarded the crystallization of ZrO_2 (Table 1).

The Ni/ZrO_2 and Co/ZrO_2 (Fig. 1) catalysts exhibited an additional, rather weak exothermic peak at a temperature below that of the glow exotherm. These peaks may have resulted from conversion of Co/ZrO_2 into cobalt oxide (Co_3O_4), the phase change in which occurs above 125 °C [30], and from a similar process leading to higher nickel oxides in Ni/ZrO_2 [31].

All solids evolved similarly as regards weight loss. Thus, they exhibited an initial constant loss associated to water with a DTG profile centred at *ca.* 100 °C, followed by a less marked loss ending – Co/ZrO_2 excepted – at about 500–600 °C, where signals levelled off. The percent mass loss was virtually identical (10–11%) for all impregnated solids and greater than in ZrO_2 (6%). The losses in ZrO_2 were due to physisorbed water, dehydration of hydroxyl surface groups and surface-adsorbed carbonaceous species. The impregnated catalysts additionally lost chlorinated species – as hydrochloric acid, mainly.

The presence of chlorinated species, potentially removed as volatile species such as HCl, on the surface of the catalysts led us to operate at both 200 °C – the temperature used in previous studies – and at 150 °C in order to minimize the losses of such species.

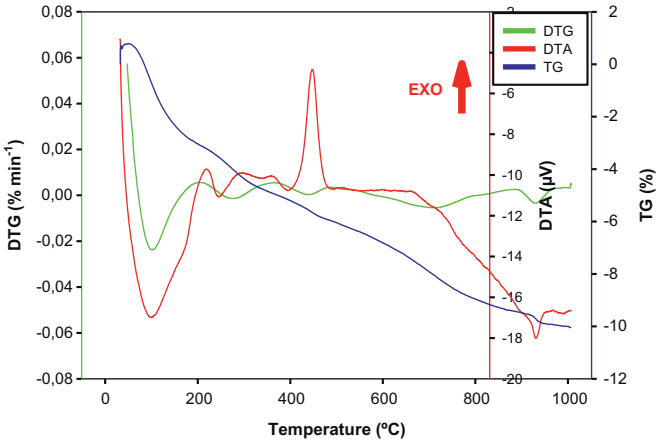

Fig. 1. TGA–DTA profile obtained in synthetic air for the Co/ZrO_2 catalyst.

Table 2
Surface atomic concentration (mole, %), as determined by XPS, for fresh and used catalysts.

Catalyst	Temp. (°C)	Oxygen (mole, %)		Carbon (mole, %)		Metal (mole, %)		Zirconium (mole, %)		Chlorine (mole, %)	
		Fresh	Used	Fresh	Used	Fresh	Used	Fresh	Used	Fresh	Used
Au/ZrO_2	150	44.6	50.6	24.1	20.0	2.8	2.4	25.7	26.3	3.0	0.61
Co/ZrO_2		52.0	48.7	18.4	23.0	1.8	1.6	25.8	25.0	2.1	0.56
Ni/ZrO_2		52.0	–	17.3	–	1.7	–	26.3	–	2.7	–
Zn/ZrO_2		53.6	–	12.0	–	2.8	–	28.3	–	3.7	–
Au/ZrO_2	200	54.1	48.4	13.2	25.5	2.4	0.8	28.1	25.3	2.7	n.d.
Co/ZrO_2		52.6	49.5	17.4	23.0	1.7	1.9	26.0	25.6	2.4	n.d.
Ni/ZrO_2		54.2	50.7	13.5	22.8	1.4	1.2	28.2	25.3	2.5	n.d.
Zn/ZrO_2		54.4	47.2	7.6	28.4	4.1	2.2	29.5	22.1	4.5	n.d.
ZrO_2		54.1	49.3	17.5	24.2	–	–	28.4	26.5	–	–

3.2. Chemical composition of the catalysts

Table 1 shows the impregnated metal-to-zirconium (Mt/Zr) mole fractions obtained with the three quantitation techniques used: ICP-MS, EDX and XPS.

The concentrations of impregnated species measured with ICP-MS were, in general, lower than those provided by EDX by effect of the latter being a primarily surface analysis technique and the former examining each solid as a whole; this testifies to the strong surface component of the impregnation process.

Based on the data of Tables 1 and 2, the Zn/ZrO_2 solid contained a greater proportion of impregnated metal than the others (*viz.*, a 15% Mt/Zr ratio as determined by ICP-MS). The synthetic conditions were adjusted to obtain 2 mmol of metal chloride per gram of support, equivalent to about a 25% molar concentration of metal chloride (1 mol chloride per 4 mol ZrO_2). Therefore, based on ICP results only Zn was incorporated in a near-theoretical proportion into the zirconium oxide – Co, Au and Ni were incorporated to a lower extent. According to ICP-MS results, the Au/ZrO_2 solid contained an abnormally low concentration of gold with ICP-MS, possibly as a result of the reduction to metal gold and precipitation in the acid solution prior to measurement.

In stoichiometric terms, the concentration of chloride ions in the impregnated solids should have been much higher than suggested by the XPS values (compare chlorine and metal % in Table 2). Probably, the thermal treatments removed most impregnated chlorinated species or the impregnation process was poorly efficient for such species.

3.3. Structural characterization

All catalysts were examined by X-ray diffraction (XRD) spectroscopy. Their XRD patterns were very similar and suggestive of an amorphous structure. By exception, the pattern for Au/ZrO_2 (Fig. 2) exhibited two peaks superimposed on the amorphous profile obtained for all solids. The two peaks appeared at 2θ 44.53° and 51.89°, and corresponded to the 111 and 200 reflections, respectively, in the crystal structure of cubic gold [32]. The particle size of Au/ZrO_2 was determined by applying the Scherrer equation to the two peaks in its XRD pattern and found to be 25 nm.

Based on the nitrogen adsorption isotherms, the surface area of the impregnated solids was in the region of 200 m^2/g (Table 1) and lower than that of ZrO_2 (237 m^2/g). This further confirms that impregnation was largely a surface phenomenon and clogged pores in zirconium oxide, thereby reducing its surface area.

Consistent with the XRD patterns, the FT-Raman spectra for ZrO_2, Zn/ZrO_2 and Ni/ZrO_2 lacked structurally relevant signals. On the other hand, the Raman spectra for Au/ZrO_2 and Co/ZrO_2 contained well-defined signals. Thus, the spectrum for Au/ZrO_2 (Fig. 3) exhibited two peaks at 354 and 320 cm^{-1} corresponding to the ν(Au–Cl) vibration [33]; which confirmed the presence of Au–Cl species. Based on the XRD pattern for Au/ZrO_2, gold in this solid was in the form of well-defined surface-deposited particles; however, this does not exclude an Au–Cl interaction – which was indeed confirmed by the FT-Raman spectrum.

The Raman spectrum for $Co/ZrO_2$200 (Fig. 3) exhibited three well-defined peaks at 688, 481 and 191 cm^{-1} corresponding to the

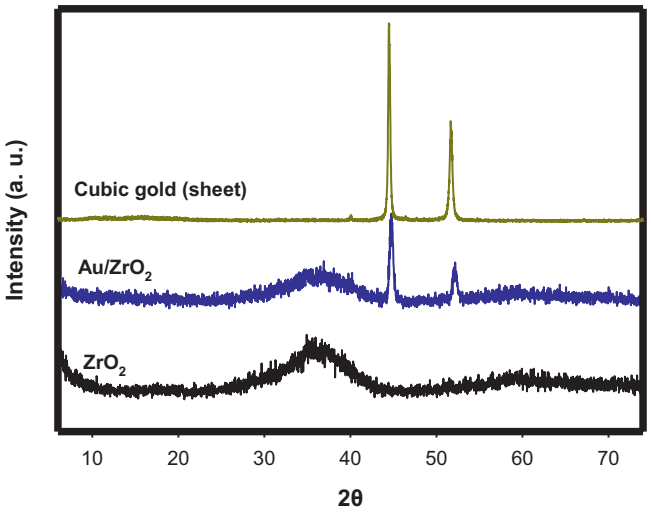

Fig. 2. XRD profiles obtained for the ZrO_2 and Au/ZrO_2 catalysts. Cubic gold pattern is also presented for comparison.

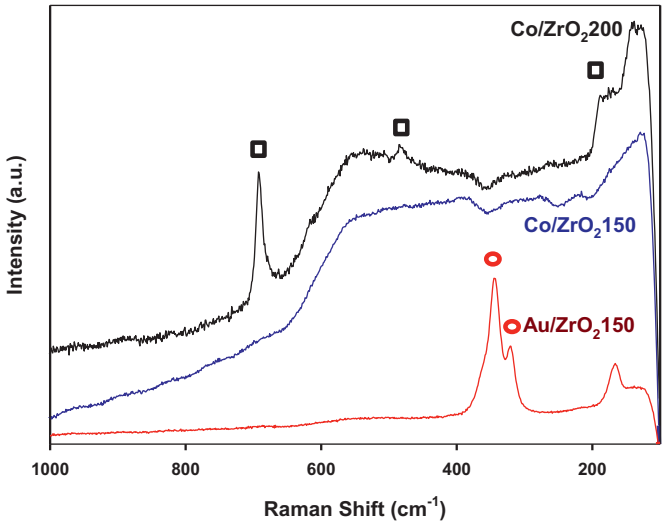

Fig. 3. FT-Raman spectra corresponding to the $Co/ZrO_2$150, $Co/ZrO_2$200 and Au/ZrO_2 catalysts. (□) Co_3O_4 [34,35]; (○) Au–Cl interaction [33].

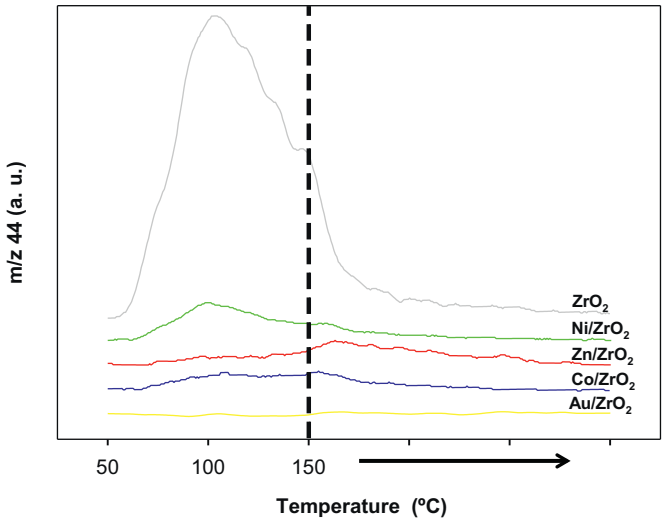

Fig. 4. Profiles obtained in the temperature-programmed desorption of CO_2 for the catalysts treated at 150 °C.

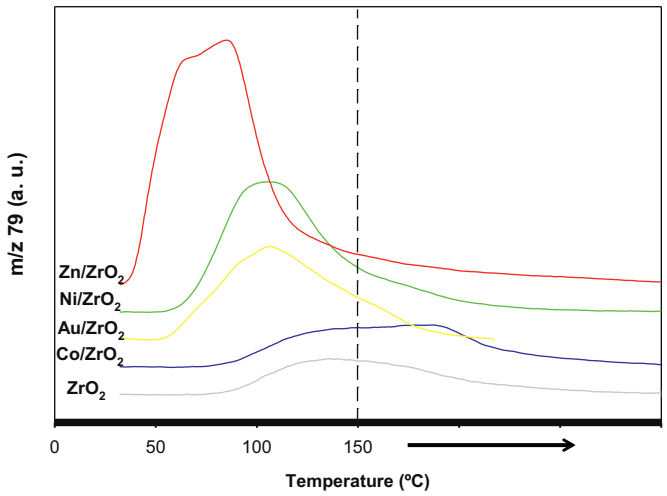

Fig. 5. Profiles obtained in the temperature-programmed desorption of pyridine for the catalysts treated at 150 °C.

A_{1g}, E_g and F_{2g} symmetry bands, respectively, in Co_3O_4 [34,35]. On the other hand, the spectrum for $Co/ZrO_2$150 (Fig. 3) contained no peak, which indicates that cobalt present in this solid underwent a phase change between 150 and 200 °C leading to the formation of Co_3O_4 as previously revealed by the thermogravimetric analysis.

The XPS technique was used to study the impregnated metals in addition to Zr, O, Cl and C – the last was present as surface-adsorbed carbon atmospheric species in all solids (adventitious carbon) (Table 2).

All impregnated catalysts exhibited two XPS peaks at 182 and 184 eV that were unequivocally assigned to the $3d_{5/2}$ and $3d_{3/2}$ band, respectively, for zirconium. These energy values are consistent with those for the ZrO_2 solid and also with previously reported values for zirconium oxide [36]. Therefore, the XPS results provided no evidence of a potential interaction between surface zirconium and other elements by effect of impregnation.

Oxygen exhibited a similar XPS profile in all solids. The O1s signal was asymmetric, which suggests the presence of various oxygen species including Zr^{4+}-bound oxygen, hydroxyl surface groups and highly oxidized carbonaceous species.

The presence of chloride in the solids was confirmed by a signal at *ca.* 269–270 eV, typical of Cl2s in metal chlorides [37], in their profiles.

The binding energies for the impregnated metals were slightly higher than reported values, which can be ascribed to the presence of oxygen and chlorine on the surface of the solids. In fact, $Co/ZrO_2$200 and $Ni/ZrO_2$200 may even have contained trivalent cations. The TGA–DTA results were suggestive of the presence of these species, which was confirmed by the consistency of the FT-Raman spectrum for Co/ZrO_2 with the presence of Co_3O_4. Also, the similarity in Cl2s binding energies between the impregnated solids is suggestive of metal–Cl interactions in all.

3.4. Surface acid–base properties

3.4.1. Basicity

Fig. 4 shows the CO_2 temperature-programmed desorption profiles (TPD-CO_2) for the catalysts heated at 150 °C and Table 1 lists the basicity values obtained from the profiles in μmol of CO_2 adsorbed per gram and per m^2 of catalyst. Overall, the impregnated catalysts were scarcely basic. Also, Ni/ZrO_2 was slightly more basic than Zn/ZrO_2, which was followed in this respect by Co/ZrO_2 and, finally, Au/ZrO_2 as the least basic solid. By contrast, the starting zirconium oxide was roughly one order of magnitude more basic than the impregnated solids. The lower basicity of the impregnated catalysts may have resulted from interactions between the metal cations (Lewis acids) and basic sites in zirconium oxide during the impregnation process [28].

3.4.2. Acidity

Fig. 5 shows the pyridine thermal programmed desorption profiles for the catalysts heated at 150 °C and Table 1 the corresponding acidity values in μmol pyridine/g and μmol pyridine/m^2. The profiles allow the catalysts to be classified into two groups, namely: Zn/ZrO_2, Ni/ZrO_2 and Au/ZrO_2 on the one hand; and ZrO_2 and Co/ZrO_2 on the other.

As can be seen from Fig. 5, the profiles for the former group of solids indicates that PY desorption started at a low temperature and rapidly peaked as is typical for weak acid sites. Worth special note in this group is Zn/ZrO_2, which contains many more – albeit weaker – acid sites than the others; this is consistent with the high surface concentration of Zn detected in it.

Co/ZrO_2 and ZrO_2 exhibited virtually identical profiles with an increased acidity component that was absent from the other solids. The presence of cobalt enhanced this component in zirconium oxide.

The catalysts heated at 200 °C were also subjected to TPD-PY tests and found to possess higher acidity than those heated at 150 °C (see Table 1). This was especially so with Co/ZrO_2 and Ni/ZrO_2, which were nearly as acidic as Zn/ZrO_2. The last was the solid with the highest acidity and ZrO_2 the catalyst with the lowest (expressed as μmol PY/m^2).

In summary, ZrO_2 is a solid with a high concentration of basic sites and a low concentration of medium-strength acid sites. Impregnating it with metal chlorides dramatically reduced its surface basicity and markedly increased its proportion of low-strength acid sites – by exception, Co/ZrO_2 exhibited a slight increase in acid sites of moderate strength.

In order to acquire a deeper knowledge of the type (Brønsted or Lewis) and distribution of surface acid sites in the catalysts, we used diffuse reflectance Fourier transform infrared (DRIFT) spectra and pyridine as probe molecule. All impregnated catalysts except Au/ZrO_2 exhibited a similar spectral profile (Fig. 6). Thus, the DRIFT spectra contained a very strong peak at 1445 cm^{-1} corresponding to pyridine adsorbed at Lewis sites, a much weaker peak at 1486 cm^{-1} previously assigned to both Brønsted and Lewis sites, and a third peak at 1600–1615 cm^{-1} which was difficult to assign because both

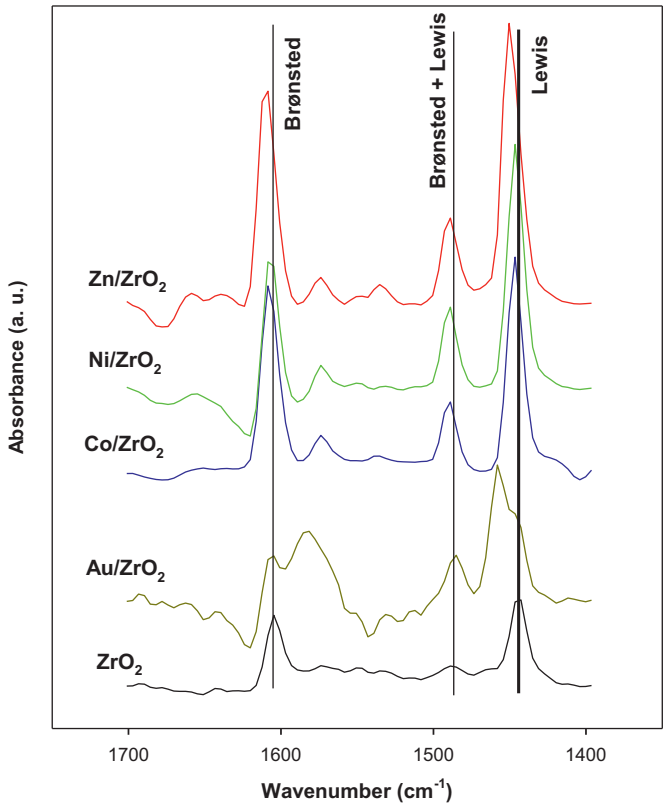

Fig. 6. Diffuse reflectance infrared Fourier transformed spectra (DRIFT) of the catalysts saturated with pyridine at 150 °C. The bands assigned to pyridine interacting with Brønsted and Lewis acid sites are indicated.

Brønsted and Lewis acid sites exhibit bands in this wavenumber range (at 1611 cm^{-1} the former and 1604 cm^{-1} the latter [38]). We previously detected Brønsted sites in zirconium oxides prepared with the same procedure, and therefore that component was assigned to Brønsted acid sites [27,39].

Au/ZrO_2 exhibited two peaks at 1458 and 1582 cm^{-1} in addition to the previous ones. The peak at 1458 cm^{-1} was partly overlapped with that peak at 1445 cm^{-1} and probably due to the presence of a second type of Lewis acid sites; according to Wan et al. [38], the peak at 1582 cm^{-1} is also due to Lewis acid sites. Unlike the other, common peaks, these two changed in intensity with temperature. Also, unlike the other solids, Au/ZrO_2 was previously found by FT-Raman spectroscopy to exhibit an interaction between the impregnated metal and chloride ion. This led us to assign the additional acidity of Au/ZrO_2 to the presence of large gold particles on the solid surface, the interaction of which with chloride – confirmed by FT-Raman spectroscopy – probably plays a prominent role.

The DRIFT spectroscopic results revealed the presence of Lewis acid sites in all solids, and their proportions in the impregnated catalysts to exceed that in the starting ZrO_2 solid, whose signal at 1445 cm^{-1} was the weakest among all catalysts. Also, because the intensity of DRIFT signals is proportional to acidity, the acidity sequence for the catalysts coincided with that for the TPD-PY values, with Zn/ZrO_2 exhibiting the highest acidity and ZrO_2 the lowest (Table 1).

3.5. Meerwein–Ponndorf–Verley reduction of crotonaldehyde

The MPV reduction of crotonaldehyde in the gas phase with propan-2-ol as hydrogen donor was conducted at 150 and 200 °C. Table 3 shows the catalytic activity results obtained at the two temperatures and Fig. 7 a typical reaction profile corresponding to the reaction with Au/ZrO_2 as the catalyst.

Despite the considerable differences in performance between catalysts, the reaction exhibited medium–high conversion values and a high selectivity towards but-2-enol. However, the activity virtually invariably dropped through deactivation of the catalyst and crotonaldehyde conversion fell after 5 h of reaction to variable extent depending on the particular reaction temperature and catalyst. In any case, the selectivity towards but-2-enol remained at 60–90% with all catalysts and even increased slightly as the reaction progressed (see Fig. 7).

Catalytic activity in the MPV reaction has been unambiguously related to acid sites [28] and shown to increase with increasing acidity. There is also evidence, however, that catalysts containing strong surface acid sites (Lewis sites, largely) are initially very active but undergo strong deactivation in the process [28,40].

3.5.1. MPV reduction at 150 °C

Impregnating ZrO_2 with the metal chlorides markedly increased its catalytic activity. Thus, the initial (50 min) but-2-enol yield was much higher with the impregnated catalysts than with the starting solid (19–43% *versus* 10%). As noted earlier, however, all catalysts underwent considerable deactivation (especially Co/ZrO_2 and Ni/ZrO_2, which became virtually inactive within 300 min of reaction). On the other hand, Au/ZrO_2 and Zn/ZrO_2 lost catalytic activity but provided but-2-enol yields in the region of 20% after 5 h of reaction. The but-2-enol yield after 300 min at 150 °C decreased in the following catalyst sequence: $Au/ZrO_2 > Zn/ZrO_2 \gg ZrO_2 \gg Ni/ZrO_2 > Co/ZrO_2$.

3.5.2. MPV reduction at 200 °C

Contrary to the expectations, the but-2-enol yield was not always increased by an increase in reaction temperature. Thus, Co/ZrO_2, Ni/ZrO_2 and ZrO_2 performed similarly at 200 °C, with yields about 45% that decreased as the reaction progressed. On the other hand, Au/ZrO_2 and Zn/ZrO_2 exhibited a substantially lower (about 25%) initial activity though in the case of Au/ZrO_2, it retained virtually its whole initial activity and was, together with ZrO_2, the best performing catalyst after 5 h of reaction. The reactivity (but-2-enol yield) sequence for the catalysts after 5 h of reaction at 200 °C was as follows: $ZrO_2 \approx Au/ZrO_2 > Ni/ZrO_2 > Co/ZrO_2 > Zn/ZrO_2$.

Worth special note here is the fact that, in contrast to its performance at 150 °C, ZrO_2 was the solid providing the best results at 200 °C. This is consistent with our previous results showing that optimum catalytic performance of zirconium oxide was obtained at reaction temperatures of *ca.* 200 °C [27]. Finally, catalytic

Table 3
Catalytic performance for MPV reaction of crotonaldehyde of fresh (first cycle) and reused (second cycle) catalysts as expressed as but-2-en-1-ol yield.

Catalyst	First cycle – 150 °C (yield, %)			Second cycle – 150 °C (yield, %)			First cycle – 200 °C (yield, %)			Second cycle – 200 °C (yield, %)		
	50 min	150 min	300 min	50 min	150 min	300 min	50 min	150 min	300 min	50 min	150 min	300 min
Au/ZrO_2	43.2	31.1	20.9	16.2	12.2	6.9	22.9	21.6	20.5	26.4	16.1	9.8
Co/ZrO_2	41.2	12.2	0.6	2.8	0.0	0.0	46.2	28.4	14.6	36.4	17.4	11.4
Ni/ZrO_2	18.7	6.5	1.2	2.4	0.4	0.0	42.3	25.8	17.4	30.5	19.3	12.1
Zn/ZrO_2	31.6	22.9	19.1	17.0	13.0	3.8	26.2	16.1	11.5	11.5	6.2	3.4
ZrO_2	9.9	7.0	5.6	6.6	4.2	0.0	44.1	29.9	21.6	48.2	40.3	33.3

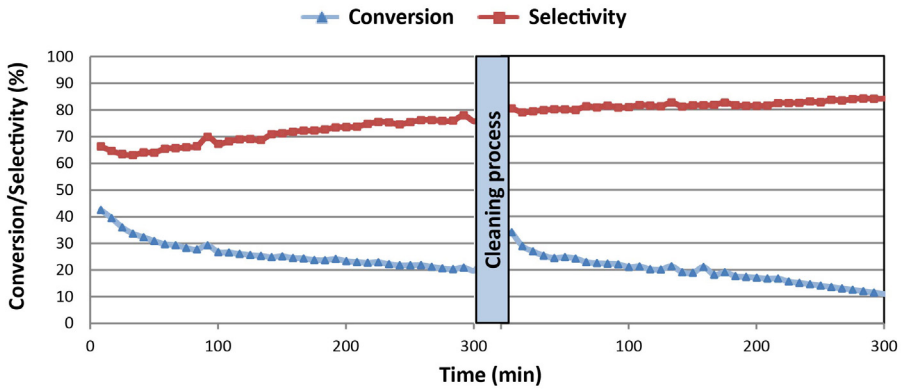

Fig. 7. MPV reduction of crotonaldehyde over the $Au/ZrO_2$200 catalyst. Crotonaldehyde conversion and selectivity to buten-2-ol obtained during the first and second reaction cycles (5 h on stream each). Between reaction cycles the catalyst was cleaned by treatment with synthetic air at the reaction temperature.

performance of Au/ZrO_2 at 150 °C is particularly interesting, with 21% yield in but-2-enol after 5 h.

3.6. Deactivation of the catalysts

A deeper study of the catalyst deactivation process at the two temperatures provided interesting information about catalytic performance. Fig. 8 shows the percent activity loss for each catalyst after 5 h of reaction at 150 and 200 °C.

As stated above, all catalysts lost much of their activity at both temperatures, but especially at 150 °C. This was particularly apparent in Co/ZrO_2 and Ni/ZrO_2, with which the initial crotyl alcohol yield fell by 99 and 94%, respectively. In any case, these two solids were also those exhibiting the greatest deactivation at 200 °C: 68 and 59%, respectively. Pure ZrO_2 performed similarly, with an activity loss of 40–50% at both temperatures. Finally, Au/ZrO_2 lost 52% of its activity at 150 °C but only 10% at 200 °C and was thus the best overall performer as regards retaining catalytic activity.

If the catalytic activity exhibited by the metal impregnated catalysts at the lower temperature is associated with their Lewis acidity (Figs. 5 and 6, Table 1), then one can assume catalytic deactivation at that temperature to be the result of (a) the destruction of Lewis acid sites caused by decomposition of impregnated active species or (b) the irreversible adsorption of reactants or products or deposition of carbonaceous species formed at the acid sites. The dissimilar behaviour of the catalysts as regards deactivation at 150 and 200 °C can provide valuable clues to identify the process involved in each case. Thus, increased deactivation at 150 °C is suggestive of destruction of acid sites produced by impregnation of the solids

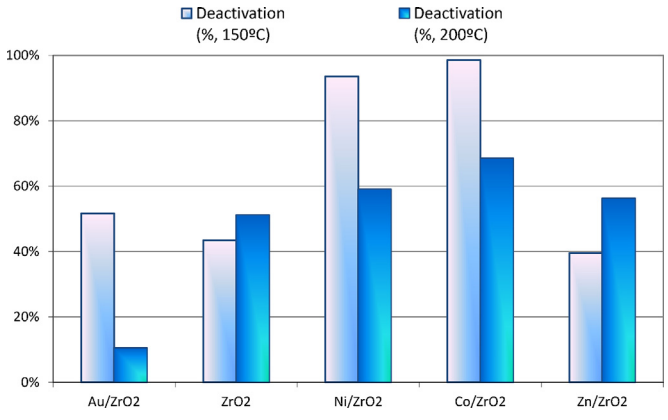

Fig. 8. Deactivation of the catalysts in the gas-phase MPV reduction of crotonaldehyde at 150 and 200 °C. Catalytic activity lost (%) along the first 5 h of reaction.

since deposition of carbonaceous species is more likely at higher temperatures. Also, heating the catalysts at 200 °C prior to the reaction was found to partially destroy impregnated chloride species – at least in $Co/ZrO_2$200, the FT-Raman spectrum for which (Fig. 3) was consistent with the presence of Co_3O_4. This phase change is probably highly influential on the catalytic activity of this solid.

Finally, deactivation at 200 °C should largely be the result of the formation of adsorbed species at acid sites in the catalysts. In any case, a deeper study of the deactivation process and characterization of the deactivated solids will be required to draw accurate conclusions in this respect.

3.7. Regeneration of the catalysts

After a 5 h reaction cycle, the catalysts were cleaned up *in situ* by passing an air stream at the reaction temperature (150 or 200 °C) and subjected to a second 5 h reaction cycle (Fig. 7).

As can be seen from Table 3, the catalysts tested at 150 °C hardly recovered their activity; thus, the activity at the start of the second cycle was similar to that at the end of the first. In fact, deactivation continued through the second cycle and only Au/ZrO_2 and Zn/ZrO_2 remained active after 10 h of reaction, with a yield of 7 and 4%, respectively.

The clean-up runs performed at 200 °C revealed another difference between catalysts. Thus, Zn/ZrO_2 only recovered their activity scarcely while for Co/ZrO_2, Ni/ZrO_2 the activity recovered to an extent approaching the initial level (at 50 min). Finally, the less deactivated Au/ZrO_2 system recovered its initial activity upon regeneration treatment. In the second reaction cycle, the catalysts performed similarly to the first, with a but-2-enol conversion at 300 min slightly lower than one-half the initial value (at 50 min). Finally, ZrO_2 provided the best results in the second cycle, with conversions slightly exceeding those of the first.

3.8. TGA–MS analysis of the spent catalysts

Using the TGA in combination with mass spectrometry provided additional useful information to examine the deactivated catalysts after the reaction (see Fig. 9).

All catalysts exhibited a TGA–MS profile in synthetic air very similar to that of Fig. 9A. Thus, all gave a strong exothermic peak starting slightly below 200 °C and ending at 400–500 °C depending on the particular catalyst. This exothermic process was accompanied by a weight loss of 5–7% from all catalysts – by exception, Zn/ZrO_2 lost 14%. In some solids, this signal was overlapped with the above-mentioned glow exotherm (410–460 °C), but both signals were clearly distinguished in most profiles.

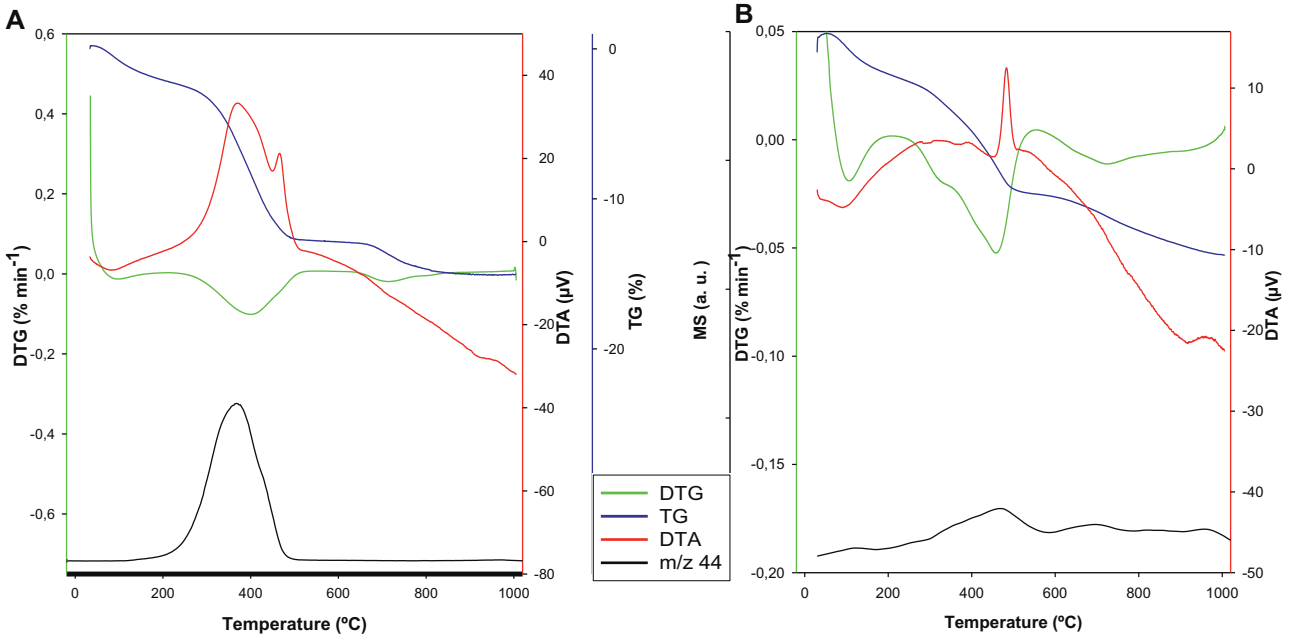

Fig. 9. TGA–MS profile obtained for the used $Zn/ZrO_2$150 catalyst in (a) synthetic air and (b) argon flow.

The exothermic signal was no doubt due to combustion of carbon compounds depositing onto the surface of the catalysts during the reaction. This was especially apparent from the similarity between the MS signal for carbon dioxide (m/z 44) and the exothermic peak in the TGA profile (Fig. 9A), the latter being absent from the TGA profiles for the fresh catalysts.

The differences in activity between the previously used catalysts in the second reaction cycle can be explained on the basis of these results. As stated above, the combustion of surface carbonaceous deposits occurred over the temperature range 180–460 °C, the specific temperature differing between catalysts. These results would point out to non graphitized carbonaceous deposits consistent with the development of a hydrocarbon pool (soft-coke) which burns at temperatures lower than 500 °C [41,42]. This suggests that deactivation of the solids was a result of the surface adsorption of carbonaceous species. As confirmed by the experimental results, clean-up between reaction cycles at 150 °C had little effect on surface carbonaceous deposits, so no much catalytic activity was recovered (Table 3).

The TGA–MS profiles obtained in an inert (argon) atmosphere varied widely from those obtained in synthetic air. No relationship between the mass (m/z 44) and TGA profiles for the reused catalysts was found, in this case (see Fig. 9B). Obviously, no surface organic matter can have burnt and heat flow (DTA profile) been produced as a result in the absence of oxygen. However, the fresh ZrO_2 solid exhibited an identical profile and desorbed a large amount of CO_2 (not shown). This phenomenon was seemingly the consequence of the high surface basicity of ZrO_2 and its retaining CO_2 as a result (see Table 1 and Fig. 4).

Although no combustion was observed, monitoring the species involved in the reaction by MS revealed that many were retained on the catalyst surface and released as the temperature was raised. All catalysts released water and some CO_2 during their TGA–MS analysis – by exception, Au/ZrO_2 released none of the monitored species, which testifies to their low surface adsorption capability. Like Zn/ZrO_2 and Ni/ZrO_2, ZrO_2 and Co/ZrO_2 again had similar profiles for the different m/z signals. In addition to water and CO_2 evolution (the last being related to catalyst basicity) there is a broad desorption peak in the MS profile (total ion chromatogram, not shown) at 400–500 °C, related to the presence on the catalyst surface of carbonaceous deposits. It is then assumed that strong adsorption and/or polymerization of reactants and/or reaction products or byproducts formed during the MPV reduction of crotonaldehyde could be responsible for the formation of those carbonaceous deposits that finally lead to catalyst deactivation.

3.9. Characterization of spent catalysts

Tables 2 and 4 show the results of the characterization of the catalysts previously used in the MPV reaction.

The XPS profiles for the spent catalysts were essentially similar to those for the fresh catalysts (Table 2). However, all analyzed re-used solids except $Au/ZrO_2$150 exhibited an increased amount of surface carbon, which confirms the presence of carbonaceous species affecting catalytic activity. The catalysts were not analyzed for chlorine because fouling detracted considerably from the sensitivity of the tests.

Table 4
Gas-phase MPV reduction of crotonaldehyde at 150 °C. Some textural (N_2 isotherms), structural (TGA–DTA) and chemical surface (acidity, TPD of pyridine) characteristics of used catalysts (5 h on stream).

Used catalyst	BET (m^2/g)	Pore Ø (A)	T_G (°C)	Acidity (µmol PY/g)		Acidity (µmol PY/m^2)	
				Fresh	Used	Fresh	Used
Au/ZrO_2	155	6.1	439	11.7	7.9	0.06	0.05
Co/ZrO_2	87	8.8	464	17.0	8.1	0.08	0.09
Ni/ZrO_2	109	7.2	464	15.1	8.4	0.08	0.08
Zn/ZrO_2	56	14.2	479	19.6	7.2	0.10	0.13
ZrO_2	206	6.0	428	12.3	7.8	0.05	0.04

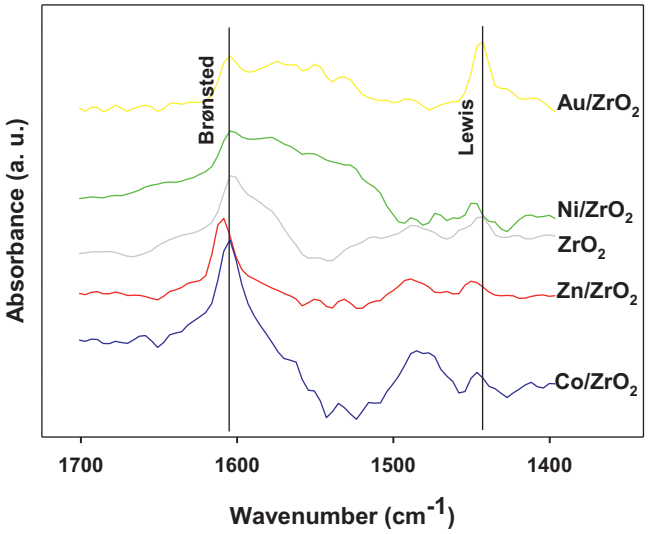

Fig. 10. Diffuse reflectance infrared Fourier transformed spectra (DRIFT) of pyridine chemisorbed on the used (deactivated) catalysts.

As expected, the re-used catalysts had a decreased surface area by effect of reactants, products and by-products being retained and clogging their pores. Zn/ZrO_2 and ZrO_2 were the solids exhibiting the greatest and smallest loss of surface area (70 and 14%, respectively). This further confirms the larger deactivation of Zn/ZrO_2 relative to the other catalysts as the likely result of its increased surface acidity – and consequently increased deposition of poisoning substances at, presumably, Lewis acid sites. On the other hand, Au/ZrO_2 was the catalyst adsorbing the smallest amounts of carbonaceous substances (20.5%) despite its possessing two different types of Lewis acid sites. We can therefore conclude that Au/ZrO_2 was less prone to adsorbing carbonaceous species, consistent with the above-described XPS data (Table 2), and the TGA–MS and surface area results (Table 4).

Like the XPS profiles, the DRIFT spectra for chemisorbed PY differed strongly between fresh and used catalysts. Profiles were much noisier and the three peaks given by the fresh catalysts reduced to one (*viz.*, that appearing at 1604–1607 cm^{-1} and assigned to Brønsted acid sites) in the re-used catalysts (Fig. 10). Thus, the DRIFT spectra for chemisorbed pyridine revealed that Lewis acidity disappeared when the catalysts were used in the MPV reduction of crotonaldehyde for 5 h. The loss of surface area and the disappearance of Lewis acid sites are two solid enough reasons to believe that deactivation of the catalysts was mostly the result of poisoning of their Lewis acid sites by carbonaceous deposits.

Worth special note here are the results for Au/ZrO_2. As noted earlier, this was the only catalyst containing different types of Lewis acid sites, probably as a result of the presence of Au metal particles (see the XRD patterns in Fig. 2) interacting with chlorinated species (see FT-Raman spectra in Fig. 3). Unlike the other catalysts, Au/ZrO_2 retained the peak at 1445 cm^{-1} associated to Lewis acidity in the DRIFT spectrum for chemisorbed pyridine (Fig. 10). This, together with the lower surface area lost upon use in the MPV reaction (Table 4), suggests that Au/ZrO_2 was less markedly deactivated and hence retained a greater amount of catalytic activity after 5 h reaction (Table 4) by effect of this type of acid sites being less prone to deactivation [9,43].

Finally, the thermal programmed desorption profiles for pyridine up to 200 °C were very similar for all catalysts, so they afford no individual conclusions. The amounts of pyridine desorbed in μmol/g were similar between solids, but differed markedly when expressed in μmol/m^2 (Table 4). The most interesting conclusion here is that the amount of pyridine desorbed per unit surface area was virtually identical between fresh and used catalysts even though most lost a large amount of surface. Therefore, the catalysts retained their ability to adsorb pyridine in spite of their dramatically reduced surface area (Table 4). The most plausible explanation for these results is that the surface deposits produced by the reaction do not affect all active sites identically. If one bears in mind that the DRIFT-PY spectra reflected disappearance of Lewis acid sites, then these sites must have been those undergoing the greatest fouling and hence the fastest deactivation. Based on their rapid initial deactivation, Lewis acid sites in the catalysts must possess an increased catalytic activity that decreases as they are deactivated by effect of the deposition of carbonaceous residues. Such residues probably block pore access and reduce the surface area of the solids; however, unblocked sites are bound to retain their ability to adsorb pyridine irrespective of their nature or strength. As a result, the acidity per unit area must remain fairly constant if one assumes the number of active surface sites to be uniform.

As noted earlier, selectivity increased as the MPV reaction progressed with all solids (Fig. 7). The increase can be ascribed to Brønsted acid sites, the significance of which increases as the reaction develops since, based on the DRIFT-PY results, they are less prone to deactivation.

4. Conclusions

The catalysts prepared in this work possess medium catalytic activity in the MPV reduction of crotonaldehyde. Impregnating the starting zirconium oxide with various metal chlorides increased its catalytic activity at the lower temperature studied (150 °C), but not at the higher (200 °C). In any case, all solids exhibited deactivation to a variable extent.

Overall, the solids impregnated with a metal chloride behaved in two different ways at 150 °C. On the one hand, Au/ZrO_2 and Zn/ZrO_2 exhibited slow, sustained deactivation throughout the reaction and low recovery of their catalytic activity by air treatment at 150 °C. On the other, Co/ZrO_2 and Ni/ZrO_2 almost completely deactivated after 5 h on stream. For reactions performed at 200 °C, Co/ZrO_2 Ni/ZrO_2 and Zn/ZrO_2 exhibit a similar trend with a loss in activity of over 50% after 5 h whereas again deactivation is lower for Au/ZrO_2. A remarkable improvement in catalytic performance of ZrO_2 was achieved on increasing the reaction temperature from 150 °C up to 200 °C which is consistent with our previous results.

Co/ZrO_2 underwent a phase change between 150 and 200 °C by which the cobalt was oxidized to Co_3O_4. This structural change increased surface acidity and catalytic activity in the solid at 200 °C as a result. Probably, Ni/ZrO_2 underwent similar changes which, however, could not be confirmed.

Although the catalysts contain both Brønsted and Lewis acids sites active in the MPV reduction of crotonaldehyde, the results suggest that the latter are much more active but undergo much more drastic deactivation. Despite their lower activity, Brønsted acid sites are seemingly more selective judging by the reactivity and the characterization of the spent catalysts.

Deactivation of the catalysts is a result of poisoning and fouling of their surface by deposits of carbonaceous species among the reaction products and by-products. As shown by the TGA–MS profiles for the catalysts, clean-up at 200 °C recovers a substantial portion of the initial activity in some solids by effect of partial burning of the carbonaceous residues.

Solid Au/ZrO_2 is the least prone to deactivation. The presence of Lewis acid sites undergoing no deactivation (DRIFT-PY spectra) might be related to that of Au metal particles (XRD patterns) interacting with chlorinated species (FT-Raman spectra). The low loss of surface area of this catalyst during the reaction must be a result

of a reduced surface deposition of carbonaceous species leading to less marked deactivation of acid sites in it.

All in all, a significant improvement in catalytic performance of ZrO_2 for gas-phase selective hydrogenation of crotonaldehyde to buten-2-ol at low reaction temperature (150 °C) was obtained on incorporation of metal chlorides (particularly gold) through the impregnation method.

Acknowledgments

The authors are thankful to Junta de Andalucia and FEDER funds (P07-FQM-02695, P08-FQM-3931 and P09-FQM-4781 projects) for financial support.

References

[1] K. Bauer, D. Garbe, H. Surbung, Common Fragrance and Flavor Materials: Preparation, Properties and Uses, Wiley-VCH Verlag GmbH, Weinheim, 2001.
[2] P. Maki-Arvela, J. Hajek, T. Salmi, D. Yu Murzin, Applied Catalysis A-General 292 (1–2) (2005) 1–49.
[3] J.R. Ruiz, C. Jimenez-Sanchidrian, J.M. Hidalgo, Current Organic Chemistry 11 (2007) 1113–1125.
[4] S.C. Jin, Bulletin of the Korean Chemical Society 28 (2007) 2162–2190.
[5] B. Uysal, B.S. Oksal, Journal of Chemical Sciences 123 (2011) 681–685.
[6] E.J. Creyghton, R.S. Downing, Journal of Molecular Catalysis A: Chemical 134 (1998) 47–61.
[7] D. Klomp, T. Maschmeyer, U. Hanefeld, J.A. Peters, Chemistry – A European Journal 10 (2004) 2088–2093.
[8] R. Cohen, C.R. Graves, S.B.T. Nguyen, J.M.L. Martin, M.A. Ratner, Journal of the American Chemical Society 126 (2004) 14796–14803.
[9] G.K. Chuah, S. Jaenicke, Y.Z. Zhu, S.H. Liu, Current Organic Chemistry 10 (2006) 1639–1654.
[10] M.A. Aramendía, V. Borau, C. Jiménez, J.M. Marinas, J.R. Ruiz, F.J. Urbano, Journal of Molecular Catalysis A: Chemical 171 (2001) 153–158.
[11] F. Braun, J.I. Di Cosimo, Catalysis Today 116 (2006) 206–211.
[12] J.I. Di Cosimo, A. Acosta, C.R. Apesteguía, Journal of Molecular Catalysis A: Chemical 234 (2005) 111–120.
[13] J.I.D. Cosimo, A. Acosta, C.R. Apesteguía, Journal of Molecular Catalysis A: Chemical 222 (2004) 87–96.
[14] M.A. Aramendía, V. Borau, C. Jiménez, J.M. Marinas, J.R. Ruiz, F.J. Urbano, Applied Catalysis A-General 244 (2) (2003) 207–215.
[15] Y. Zhu, S. Liu, S. Jaenicke, G.K. Chuah, Catalysis Today 97 (2004) 249–255.
[16] S. Liu, S. Jaenicke, G.K. Chuah, Journal of Catalysis 206 (2002) 321–330.
[17] Y. Zhu, G.K. Chuah, S. Jaenicke, Journal of Catalysis 241 (2006) 25–33.
[18] M. Boronat, A. Corma, M. Renz, Journal of Physical Chemistry B 110 (2006) 21168–21174.
[19] A. Ramanathan, D. Klomp, J.A. Peters, U. Hanefeld, Journal of Molecular Catalysis A: Chemical 260 (2006) 62–69.
[20] B. Uysal, B.S. Oksal, Applied Catalysis A-General 435 (2012) 204–216.
[21] P. Selvam, S.U. Sonavane, S.K. Mohapatra, R.V. Jayaram, Advanced Synthesis and Catalysis 346 (2004) 542–544.
[22] S. Nishiyama, M. Yamamoto, H. Izumida, S. Tsuyura, Journal of Chemical Engineering of Japan 37 (2) (2004) 310–317.
[23] K. Tanabe, T. Yamaguchi, Catalysis Today 20 (2) (1994) 185–197.
[24] K. Tanabe, Materials Chemistry and Physics 13 (1985) 347.
[25] C.N. Rhodes, D.R. Brown, Journal of the Chemical Society, Faraday Transactions 89 (9) (1993) 1387–1391.
[26] D. Guillaume, S. Gautier, I. Despujol, F. Alario, P. Beccat, Catalysis Letters 43 (1–2) (1997) 213–218.
[27] J.F. Miñambres, M.A. Aramendia, A. Marinas, J.M. Marinas, F.J. Urbano, Journal of Molecular Catalysis A: Chemical 338 (1–2) (2011) 121–129.
[28] J.F. Miñambres, A. Marinas, J.M. Marinas, F.J. Urbano, Journal of Catalysis 295 (2012) 242.
[29] A. Rahman, Thermochimica Acta 85 (1985) 3–13.
[30] T.N. Ramesh, Journal of Solid State Chemistry 183 (2010) 1433–1436.
[31] H.C. Zeng, J. Lin, W.K. Teo, F.C. Loh, K.L. Tan, Journal of Non-Crystalline Solids 181 (1–2) (1995) 49–57.
[32] M. Epifani, C. Giannini, L. Tapfer, L. Vasanelli, Journal of the American Ceramic Society 83 (10) (2000) 2385–2393.
[33] P.J. Murphy, M.S. Lagranje, Geochimica et Cosmochimica Acta 62 (1998) 3515–3526.
[34] S. Farhadi, J. Safabakhsh, Journal of Alloys and Compounds 515 (2012) 180–185.
[35] Y. Lou, L. Wang, Y. Zhang, Z. Zhao, Z. Zhang, G. Lu, Y. Guo, Catalysis Today 175 (1) (2011) 610–614.
[36] G.K. Chuah, S. Jaenicke, B.K. Pong, Journal of Catalysis 175 (1) (1998) 80–92.
[37] M.C. Militello, S.J. Simko, Surface Science Spectra 3 (1994) 402–409.
[38] K.T. Wan, C.B. Khouw, M.E. Davis, Journal of Catalysis 158 (1) (1996) 311–326.
[39] G. Connell, J.A. Dumesic, Journal of Catalysis 101 (1) (1986) 103–113.
[40] G. Yaluris, R.B. Larson, J.M. Kobe, M.R. González, K.B. Fogash, J.A. Dumesic, Journal of Catalysis 158 (1) (1996) 336–342.
[41] L.J. France, D.C. Apperley, E.J. Ditzel, J.S.J. Hargreaves, J.P. Lewicki, J.J. Liggat, D. Todd, Catalysis Science & Technology 1 (2011) 932–939.
[42] D. Zhang, R. Wang, L. Wang, X. Yang, Journal of Molecular Catalysis A: Chemical 366 (2013) 179–185.
[43] J.E. Bailie, H.A. Abdullah, J.A. Anderson, C.H. Rochester, N.V. Richardson, N. Hodge, J.G. Zhang, A. Burrows, C.J. Kiely, G.J. Hutchings, Journal of Physical Chemistry B 3 (18) (2001) 4113–4121.